ADVANCES IN ATMOSPHERIC SCIENCES, VOL. 32, NOVEMBER 2015, 1551–1564

Simulation of Salinity Variability and the Related Freshwater Flux Forcing in the Tropical Pacific: An Evaluation Using the Beijing Normal University Earth System Model (BNU-ESM)

ZHI Hai[1], ZHANG Rong-Hua[*2], LIN Pengfei[3], and WANG Lanning[4]

[1]*The Earth System Modeling Center and College of Atmospheric Sciences, Nanjing University of Information Science and Technology, Nanjing* 210044

[2]*Key Laboratory of Ocean Circulation and Waves, Institute of Oceanology, Chinese Academy of Sciences, Qingdao* 266071

[3]*State Key Laboratory of Numerical Modeling for Atmospheric Sciences and Geophysical Fluid Dynamics, Institute of Atmospheric Physics, Chinese Academy of Sciences, Beijing* 100029

[4]*College of Global Change and Earth System Science, Beijing Normal University, Beijing* 100875

(Received 04 November 2014; revised 18 April 2015; accepted 30 April 2015)

ABSTRACT

The climatology and interannual variability of sea surface salinity (SSS) and freshwater flux (FWF) in the equatorial Pacific are analyzed and evaluated using simulations from the Beijing Normal University Earth System Model (BNU-ESM). The simulated annual climatology and interannual variations of SSS, FWF, mixed layer depth (MLD), and buoyancy flux agree with those observed in the equatorial Pacific. The relationships among the interannual anomaly fields simulated by BNU-ESM are analyzed to illustrate the climate feedbacks induced by FWF in the tropical Pacific. The largest interannual variations of SSS and FWF are located in the western-central equatorial Pacific. A positive FWF feedback effect on sea surface temperature (SST) in the equatorial Pacific is identified. As a response to El Niño–Southern Oscillation (ENSO), the interannual variation of FWF induces ocean processes which, in turn, enhance ENSO. During El Niño, a positive FWF anomaly in the western-central Pacific (an indication of increased precipitation rates) acts to enhance a negative salinity anomaly and a negative surface ocean density anomaly, leading to stable stratification in the upper ocean. Hence, the vertical mixing and entrainment of subsurface water into the mixed layer are reduced, and the associated El Niño is enhanced. Related to this positive feedback, the simulated FWF bias is clearly reflected in SSS and SST simulations, with a positive FWF perturbation into the ocean corresponding to a low SSS and a small surface ocean density in the western-central equatorial Pacific warm pool.

Key words: freshwater flux, salinity, feedback, tropical Pacific, BNU-ESM

Citation: Zhi, H., R.-H. Zhang, P. F. Lin, and L. N. Wang, 2015: Simulation of salinity variability and the related freshwater flux forcing in the tropical Pacific: An evaluation using the Beijing Normal University Earth System Model (BNU-ESM). *Adv. Atmos. Sci.*, **32**(11), 1551–1564, doi: 10.1007/s00376-015-4240-6.

1. Introduction

Freshwater flux (FWF, defined as precipitation minus evaporation) at the air–sea interface plays a vital role in regulating the climate and hydrological cycle in the earth system. FWF, along with surface heat fluxes (HFs) and wind, control the dynamic and thermodynamic behavior of the ocean (Zhang and Busalacchi, 2009; Hackert et al., 2011). For example, FWF can directly affect ocean salinity, which plays an important role in controlling variations of the mixed layer depth (MLD) and also modulates sea surface temperature (SST) in tropical Pacific regions with heavy precipitation (Murtugudde and Busalacchi, 1998; Han et al., 2001, Thompson et al., 2006; Wu et al., 2010; Zhang et al., 2010, 2012; Ham et al., 2012; Ma et al., 2013; Zhang et al., 2014). In such regions, where there exists strong near-surface haline stratification, salinity and related FWF are known to indirectly influence the evolution of the mixed layer temperature (Rao and Sanil Kumar, 1991; Sprintall and Tomczak, 1992; Rao and Sivakumar, 1999; Howden and Murtugudde, 2001; Zhang et al., 2013; Hackert et al., 2014; Zheng et al., 2014). Knowledge of salinity and related FWF variations is crucial to understanding the ocean hydrological cycle, a key component of the climate system (Webster, 1994).

The effects of salinity and its directly related FWF forcing have recently received much attention (e.g., Delcroix et al., 2007; Cravatte et al., 2009; Zhang et al., 2010, 2012; Fujii et

* Corresponding author: ZHANG Rong-Hua
Email: rzhang@qdio.ac.cn

© Institute of Atmospheric Physics/Chinese Academy of Sciences, and Science Press and Springer-Verlag Berlin Heidelberg 2015

al., 2012; Fettweis et al., 2013; Zhang et al., 2014; Zheng et al., 2014). For example, through their influence on horizontal pressure gradients, the equatorial thermocline, and vertical stratification, FWF forcing and its related interannually varying salinity can significantly affect tropical climate dynamics and El Niño–Southern Oscillation (ENSO) (e.g., Delcroix and Hénin, 1991; Murtugudde and Busalacchi, 1998; Maes, 2000; Maes et al., 2002; Fedorov et al., 2004; Huang and Mehta, 2005). More recently, Zhang and Busalacchi (2009) and Zheng and Zhang (2012) demonstrated that salinity, and its related FWF forcing, can induce a positive feedback effect on the interannual variability associated with ENSO by modulating stratification stability in the upper ocean. Another way in which FWF and salinity affect the ocean physics is through the barrier layer process (Lukas and Lindstrom, 1991; Zheng et al., 2014).

Using a simplified coupled ocean–atmosphere model, Zhang and Busalacchi (2009) demonstrated that the changes in SST induced by FWF can impact the atmosphere in the tropical Pacific; this has the potential to modulate the interannual variability associated with the ENSO. Reexamining the sensitivity of the ocean density structure and circulation with a zonally averaged ocean model, Sévellec and Fedorov (2011) found that ocean circulation is driven by the surface buoyancy fluxes (Q_B) associated with FWF. Zheng et al. (2014) described relationships among the interannual variability of salinity, FWF, and the barrier layer in the equatorial Pacific. In particular, using a one-dimensional boundary layer ocean model, they found that the barrier layer process induced by interannual salinity anomalies around the dateline can dramatically affect the temperature fields in the upper ocean, resulting in positive feedback that acts to enhance ENSO.

These previous studies are helpful for understanding the mechanisms with which salinity and related FWF forcing can affect ENSO cycles. However, most results have been obtained from ocean-only or simplified coupled ocean–atmosphere models (e.g., Mechoso et al., 1995; Yang et al., 1999; Zhang and Busalacchi, 2009; Zhang et al., 2012); so, the effects in fully coupled ocean–atmosphere models still need further investigation. As is well known, most coupled general circulation models tend to produce the so-called double intertropical convergence zone (ITCZ) pattern over the tropical Pacific, with excessive precipitation near the dateline off the equator, often connected with overly narrow and excessive cold SST spreading into the far western Pacific (Mechoso et al., 1995; Bellenger et al., 2014; Kang et al., 2014). As the dominant component of FWF, such precipitation bias can considerably distort the FWF pattern in the equatorial Pacific and ultimately affect the reliability of the simulated SST and ENSO.

An earth system model (ESM) has been developed at the Beijing Normal University (BNU), based on several widely evaluated climate model components (Ji et al., 2014). The model, abbreviated to BNU-ESM, has been used to study mechanisms of climate change, ocean–atmosphere interactions, and climate feedback effects on interannual to interdecadal time scales. The BNU-ESM results for the preindustrial (PI) control and historical simulations of CMIP5 (Coupled Model Intercomparison Project, Phase 5) are presented to evaluate the model's performance in terms of the mean state and internal variability. We show that BNU-ESM can simulate many observed features of the earth climate system, such as the climatological annual cycle of surface air temperature and precipitation, annual cycle of tropical Pacific SST (Wu et al., 2013).

Although some progress has been made in understanding the interannual variability of salinity and related FWF through observational analyses and simulations (e.g. Ji et al., 2014), it is necessary to understand the ability of BNU-ESM in simulating salinity and related FWF. The quality of the simulated salinity and that of related ocean physical processes are important criteria for assessing coupled models. In this paper, BNU-ESM is evaluated by analyzing the effects of salinity and related FWF on oceanic physical processes in the equatorial Pacific. Using PI control time-slice experiments with the BNU-ESM, as designed for CMIP5, the effects induced by salinity and FWF forcing are investigated, with a focus on annual climatology and interannual variations. Model and reference datasets are presented in section 2. Based on diagnostic calculations and model assessments, section 3 presents a detailed systematic analysis of the relationships among the annual mean climatology and interannual variability associated with FWF forcing and salinity in the equatorial Pacific. Finally, concluding remarks are presented in section 4.

2. Model description, data and methodology

2.1. *BNU-ESM*

The structure and individual components of BNU-ESM are briefly described here, but a more comprehensive description can be found in Ji et al. (2014). BNU-ESM is a fully-coupled earth system model. Using one central coupler component (the National Center for Atmospheric Research Coupler 6.5: NCAR-CPL6.5), BNU-ESM is a coupling of four separate models that simultaneously simulate the Earth's atmosphere (the National Center for Atmospheric Research Community Atmospheric Model version 4: NCAR-CAM4), sea-ice (the Los Alamos National Lab sea ice model version 4.1: LANL-CICE4.1), land surface (the BNU Common Land Model version 3: BNU-CoLM3) and ocean (the Geophysical Fluid Dynamics Laboratory Modular Ocean Model version 4p1: GFDL-MOM4p1). Two special processes included in BNU-ESM include an ecosystem–biogeochemical module in the ocean component (the Interactive BioGeoChemical Cycles: IBGC), and an interactive carbon cycle model in the land component (the BUN Dynamic Vegetation Submodel and terrestrial carbon and nitrogen cycles based on Lund-Potsdam-Jena: the BNU-DGVM). BNU-ESM has participated in CMIP5 and provided future climate projections for the Intergovernmental Panel on Climate Change's Fifth Assessment Report.

BNU-ESM's ocean output uses a nominal latitude–longitude resolution of 1° [down to (1/3)° within 10° of the tropical domain], with a 360° (longitude) ×200° (latitude) grid. There are 50 vertical levels, with the uppermost 23 layers each about 10 m. The atmospheric output uses an Eulerian dynamical core for transport calculations, with a T42 horizontal spectral resolution (an approximately 2.81° × 2.81° horizontal grid), with 26 levels in the vertical direction.

In this paper, we select the last 100 years (model year 1450 to 2008) of the PI control simulation to examine the characteristics of the mean climatology and interannual variability (Taylor et al., 2012). The model outputs used in the study include precipitation, evaporation, sea surface net HF, ocean temperature, and salinity.

2.2. *Observational and reanalysis data*

The following observational data are compared with the model simulations: The precipitation data are from the Global Precipitation Climatology Project (GPCP) dataset (version 2), covering the period 1979–2013 and with a 2.5° × 2.5° horizontal resolution (Adler et al., 2003). The evaporation data are derived from the Objectively Analyzed Air–Sea Fluxes (OAFlux) dataset (Yu and Weller, 2007). The ocean salinity and temperature of the mean climatology field gridded data are from Array for Real-time Geostrophic Oceanography (ARGO) observations, provided by the International Pacific Research Center (IPRC)/Asia-Pacific Data-Research Center (APDRC), with monthly and long-term climatology fields spatially averaged within 1° bins at standard depths covering the period from 2005 to 2013 (Levitus, 1983). The MLD gridded data of monthly and climatological fields are also derived directly from the IPRC/APDRC ARGO data. The ocean salinity and temperature of the long-term monthly climatology field gridded data are derived from objective analysis data (EN3_v2a) offered by the Met Office Hadley Centre, which are based on various observational data, including: the World Ocean Database 2005, the Global Temperature and Salinity Profile Project, and ARGO. The data have a horizontal resolution of 1° × 1° and 42 levels in the vertical direction, with the deepest level reaching 4000 m for the period from 2005 to the present day (Guinehut et al., 2009). The net HF of monthly and long-term climatology fields at the sea surface (latent and sensible HFs and flux-related surface meteorology) are derived from OAFlux data from 1958 to the present day, 1° gridded, and the surface radiation data from the International Satellite Cloud Climatology Project from 1983 to 2009, with 2.5° resolution (Schiffer and Rossow, 1985).

2.3. *Buoyancy flux*

The Q_B field, together with HF and wind, controls the evolution of MLD, which affects the entrainment of subsurface cold water into the upper surface in the equatorial Pacific. At the surface, Q_B is the net contribution of the HF part (Q_T) and the FWF part (Q_S), which at the sea surface can be defined as (Zhang et al., 2010).

$$Q_B = \frac{\alpha \mathrm{HF}}{(\rho c_p)} + \beta S_0 \mathrm{FWF} = Q_T + Q_S \,, \tag{1}$$

where HF is the net heat flux at the sea surface (positive when the ocean is receiving heat flux), FWF $= (P - E)$ is the net freshwater flux (P is precipitation and E is evaporation; when the ocean is gaining net freshwater, FWF is positive); α is the thermal expansion coefficient, and β the haline contraction coefficient; S_0 the reference surface salinity; c_p the heat capacity of seawater, and ρ the density of seawater.

More comprehensive description and the calculation of the physical quantities about (Q_B, Q_T and Q_S) can be found in Zhang et al. (2010).

3. Results

3.1. *Annual mean climatology*

3.1.1. *Freshwater flux*

FWF at the sea surface directly affects sea surface salinity in the ocean. Therefore, it is essential that the model reproduces this forcing field realistically to simulate the ocean salinity field accurately. We begin with an analysis of the annual mean climatology, with an emphasis on the large-scale features of FWF over the tropical Pacific.

Figure 1 shows the annual mean FWF and the FWF difference between the BNU-ESM simulation and observation. The observed FWF climatology shows that the ocean mostly receives freshwater through the air–sea interface in the equatorial Pacific; the main areas with positive FWF include the equatorial Pacific Ocean and the South Pacific Convergence Zone (SPCZ), which extends southeastward in the South Pacific Ocean, with a maximum annual mean FWF of more than 4.0×10^{-5} kg m^{-2} s^{-1} (Fig. 1a). In contrast, the eastern parts of the subtropical basins in both hemispheres are major loss sites of FWF and contain the two minimum FWF centers, with annual mean values of only -3.5×10^{-5} and -4.0×10^{-5} kg m^{-2} s^{-1}.

BNU-ESM can realistically simulate some of the observed FWF features in the tropical Pacific (Fig. 1b). The ocean region receiving FWF is located in the low-latitude tropical Pacific, and the high FWF center is located near the western equatorial Pacific (i.e., the warm pool), 6.0×10^{-5} kg m^{-2} s^{-1} higher than observed. The ocean region loosing FWF is located in the eastern part of the subtropical basins in both hemispheres. The difference in precipitation is the main factor affecting the FWF in the equatorial Pacific. Figure 2 shows the annual mean climatology of precipitation from observations and the BNU-ESM simulation in the equatorial Pacific. It shows that the biases of precipitation simulated by the coupled model are mainly located along the western and eastern coasts of the tropical Pacific and in the subtropical Pacific (Fig. 2c). Due to the so-called double ITCZ in the tropical Pacific simulated by BNU-ESM (overestimated precipitation), simulated FWF into the ocean is larger than observed in the subtropical area of the southern Pacific. As a result, FWF into the ocean is low in the western subtropical

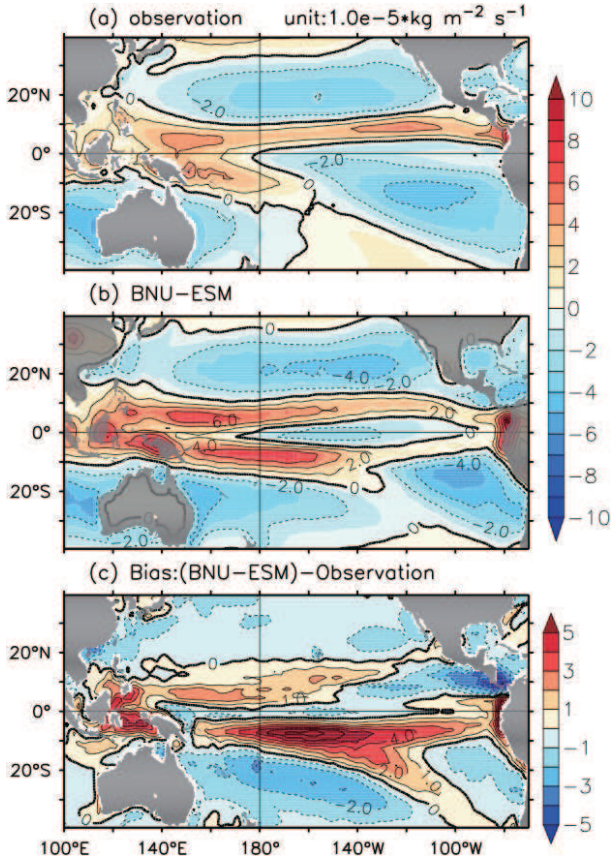

Fig. 1. Climatological annual mean FWF in the tropical Pacific: (a) GPCP observation; (b) simulated by BNU-ESM; (c) their difference (units: 10^{-5} kg m^{-2} s^{-1}; positive when downward).

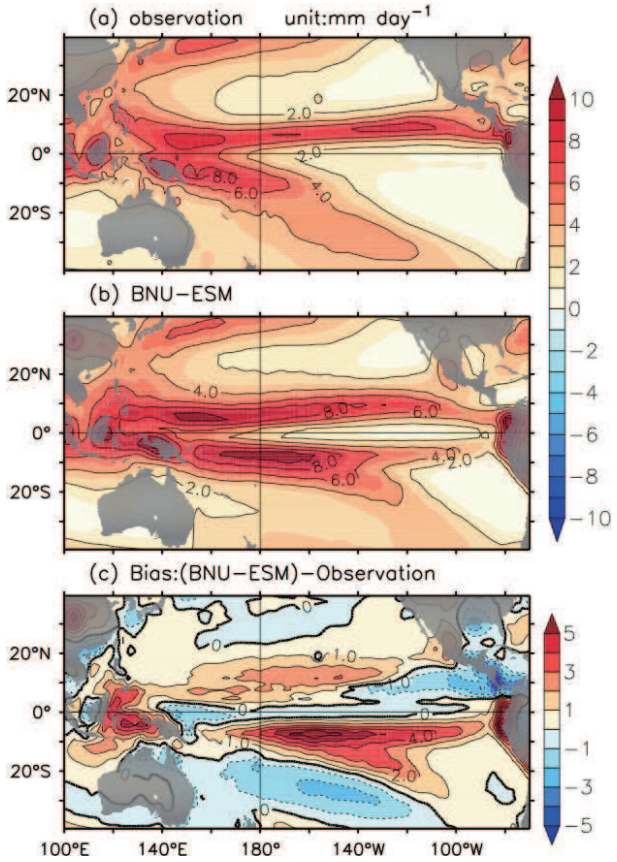

Fig. 2. Climatological annual mean precipitation in the tropical Pacific: (a) GPCP observation; (b) simulated by BNU-ESM; (c) their difference (units: mm d^{-1}).

regions of the southern Pacific. The dominance of precipitation over evaporation in the equatorial Pacific indicates that precipitation is the main contributor to FWF variability.

The differences in FWF across the air–sea interface are dominated by those in precipitation bias in the BNU-ESM simulations (Fig. 1c). Comparison of the FWF simulated by BNU-ESM with observations indicates a negative bias in the relatively narrow regions in the equatorial band, with higher FWF into the ocean between 20°S and 20°N. The main FWF biases are located in the subtropics near 10° in both hemispheres in the Pacific, with the maximum at 6.0×10^{-5} kg m^{-2} s^{-1} in the southern Pacific.

Overall, FWF simulated by BNU-ESM is larger than that observed in the southern Pacific, especially around the SPCZ. The freshwater bias mainly results from precipitation associated with the double ITCZ. Actually, based on recent research (Lin et al., 2013a, 2013b; Kang et al., 2014), the biases of surface freshwater simulated by coupled models are mainly located along the western and eastern coast of the tropical Pacific and in the subtropical Pacific, similar to the BNU-ESM simulations. Comparing the biases of BNU-ESM, the Flexible Global Ocean-Atmosphere-Land System Model, Gridpoint Version 2 (FGOALS-g2) and the Community Earth system Model-1.0 (CESM1.0), the bias of FWF is the most common phenomenon of coupled models in the Pacific due to precipitation bias. The simulated FWF is too weak in the western Pacific warm pool, too strong in the ITCZ, and too strong and extended too far east in the SPCZ. But the positive FWF bias simulated by BNU-ESM is larger than that of FGOALS-g2 and CESM1.0 in the ITCZ. As discussed in the next section, the large freshwater biases in these vast regions are closely related to sea surface salinity (SSS) simulation in the ocean.

3.1.2. *Sea surface salinity*

Ocean salinity is directly affected by FWF, one of the main factors controlling the spatial distribution of ocean density (Yu, 2011). Figure 3a shows the observed annual mean climatology of the SSS field: high salinity occurs in the subtropical convergence zones of the Northern and Southern Hemispheres, with values of 35.3 and 36.3 psu, respectively. SSS in the southern Pacific is higher than that in the Northern Hemisphere. On the other hand, low salinity represents the SPCZ and ITCZ features in the tropical Pacific. Additionally, low salinity is located in a narrow belt along the equator (namely, the warm pool and the Niño3 area in the equatorial Pacific), with a value of about 34.2; these low salinity regions reflect a response to a net input of FWF into the ocean.

The values of SSS simulated by BNU-ESM in the tropical Pacific (Fig. 3b) indicate a tendency for all simulated SSS

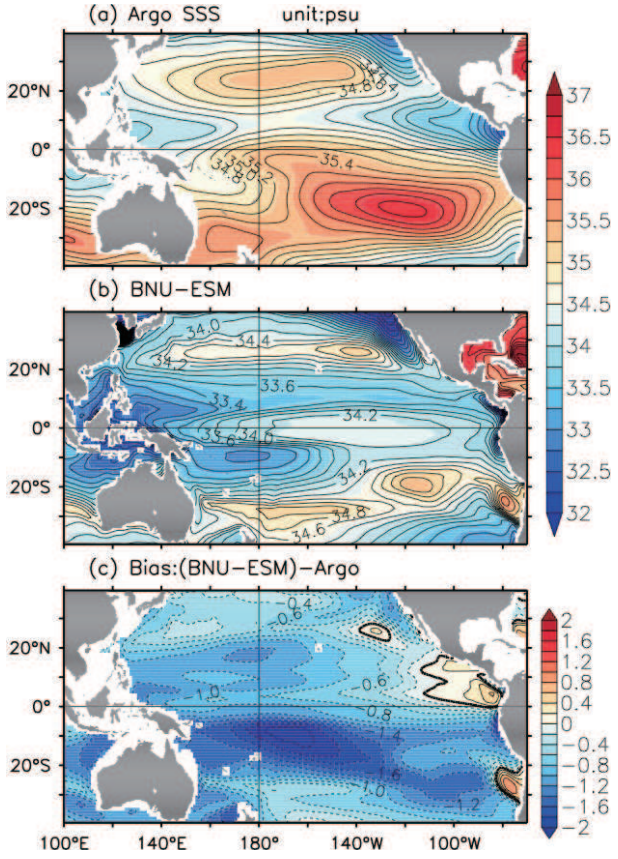

Fig. 3. Climatological annual mean SSS in the tropical Pacific: (a) ARGO observation; (b) simulated by BNU-ESM; (c) their difference (units: psu).

to be lower than observations. For example, the highest SSS value is about 35 psu in the southern Pacific. The low SSS is located in the eastern equatorial Pacific, the warm pool, and both sides along the equator. SSS displacement is in line with the heavy precipitation zone simulated by BNU-ESM, which results in lower SSS than that observed in the SPCZ and in the subtropics of the southern Pacific. Compared with observations, SSS simulated by BNU-ESM is lower in the tropical Pacific (Fig. 3c), and the largest bias is roughly 2 psu, clearly related to the double ITCZ problem that occurs in many coupled models (Lin, 2007).

There is a very close link between SSS and the local rate of FWF. Both observations and the BNU-ESM simulations share a common characteristic: there is a near linear relationship between the FWF and SSS locally, i.e., a local excess of precipitation over evaporation corresponds to low SSS. FWF is a key factor in controlling the SSS distribution in the ocean. Assuming that SSS is regulated by a one-dimensional balance between vertical advection and diffusion, the large FWF into the ocean should correspond to low SSS. The correspondence between the spatial distributions of FWF and SSS indicates that the local air–sea freshwater flux is one of the most important factors regulating salinity distribution in the upper ocean (Zhang et al., 2006).

3.1.3. *Mixed layer depth and buoyancy flux*

Next, the effects of FWF on the MLD and Q_B fields are analyzed using the annual mean climatology of observations and BNU-ESM simulations. FWF influences ocean salinity directly, and then modulates other ocean fields, such as MLD and Q_B. Relationships among these ocean fields have been discussed previously (Zhang and Busalacchi, 2009; Zheng and Zhang, 2012), in which it has been shown that the effects induced by FWF on these related physical fields indicate their intrinsic relationship with MLD and Q_B.

The FWF forcing in the equatorial Pacific tends to indirectly modulate SST in two ways. First, FWF into the ocean reduces the salinity in the western-central region, where the SST is relatively high. The decreased salinity stabilizes the upper ocean and suppresses vertical mixing at the base of the mixed layer. Second, FWF into the ocean has a direct effect on Q_B which, in turn, exerts an effect on the entrainment of subsurface water into the mixed layer and MLD. Since Q_T and Q_S tend to be opposite in sign, the effects on Q_B tend to be compensated. Thus, as part of Q_B, the FWF into the ocean acts to compensate for Q_T, leading to a less positive Q_B. Because the reduced positive Q_B tends to depress entrainment into the mixed layer, FWF into the ocean induces oceanic processes that reduce the cooling influence on the ocean surface layers in the western-central basin. These act to enhance warming conditions. Therefore, MLD and Q_B are two important physical fields associated with the FWF effect on SST in the equatorial Pacific.

Figures 4 and 5 show the annual mean climatology of MLD and Q_B for observations and the BNU-ESM simulation. Some deep mixed layer regions (deeper than 60 m) are located in the central basin and the SPCZ of the southern Pacific (Fig. 4a), while two shallow regions (shallower than 30 m) are located in the western and eastern equatorial regions in the observation. It is evident that, in the western equatorial regions, FWF into the ocean and low salinity possess a clear correspondence with MLD. For example, the shoaling of the mixed layer seen in the western Pacific can be related to low salinity. Due to the greater FWF into the ocean and lower salinity simulated by BNU-ESM in the central basin and the SPCZ of the southern Pacific, a shallower than observed mixed layer is simulated (Fig. 4c), with a difference of 20 m. Similarly, a deeper MLD is seen in the eastern equatorial Pacific and the subtropical zones of the Northern Hemisphere, where there is greater FWF out of the ocean than observed. We attribute this to the higher salinity simulated by BNU-ESM.

The Q_B is directly influenced by FWF in the equatorial Pacific, as shown in Fig. 5. The convention used in this paper is that positive Q_B is defined as an influx into the sea surface so that the sea surface layer becomes lighter (or more buoyant) with a reduced (upward) buoyant force. The Q_B is the net contribution of the FWF part (Q_S) and the HF part (Q_T). As a result, the composition of HF and FWF acts as a positive or negative source for the Q_B, to which the ocean

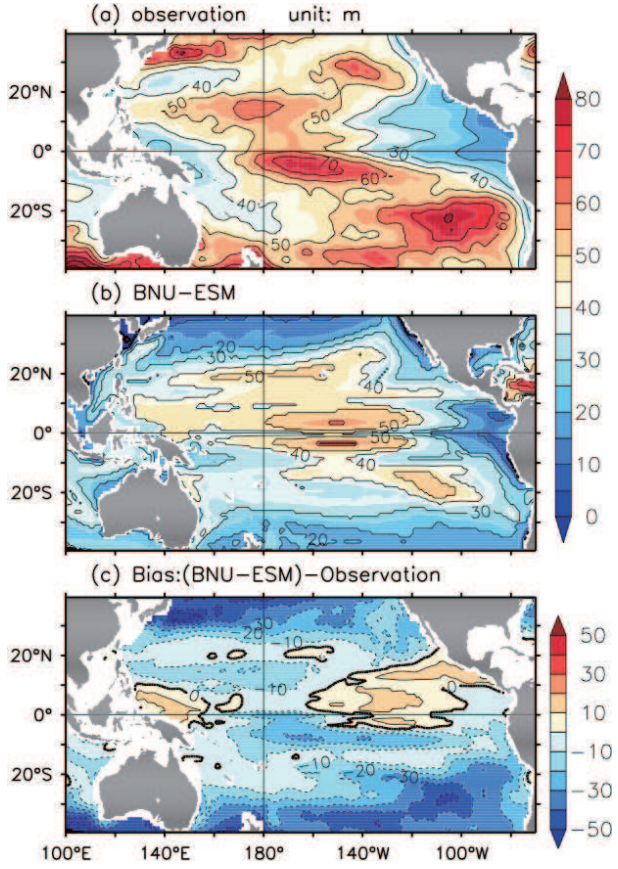

Fig. 4. Climatological annual mean MLD in the tropical Pacific: (a) ARGO observation; (b) simulated by BNU-ESM; (c) their difference (units: m).

responds through gravitational adjustment. In short, Q_B directly affects the MLD which, in turn, exerts effects on the entrainment of subsurface cold water into the mixed layer in the equatorial Pacific.

In the eastern equatorial Pacific (Figs. 5a, d and g), Q_T is the dominant contributor to Q_B but, in the western-central region, Q_S also makes a significant contribution to Q_B. Thus, as part of Q_B, FWF into the ocean acts to compensate for the positive Q_T distribution (Fig. 5g), leading to a more positive Q_B field (Fig. 5a). The increased positive Q_B tends to depress the MLD, giving rise to less entrainment of subsurface water into the mixed layer in the western equatorial Pacific. The combined effects induced by the positive Q_S distribution through the Q_B stabilize the upper layer and suppress mixing and entrainment in the upper ocean. Oceanic processes induced by FWF into the ocean surface lead to a warming effect on the surface layer in the western-central basin.

Comparison of the Q_B, Q_S and Q_T simulated by BNU-ESM with observations (Figs. 5b, e and h) shows that BNU-ESM can simulate the spatial distribution of Q_B, Q_S and Q_T climatologies in the tropical Pacific reasonably well. However, due to the FWF bias simulated by BNU-ESM, the Q_S simulated in the western tropical Pacific is higher than that observed. There are excessive compensation effects on Q_T (Fig. 5l); in particular, the positive Q_B simulated by BNU-ESM is stronger than observed in the western tropical Pacific (Fig. 5c).

3.1.4. *Climatological seasonal cycle*

As shown in Fig. 6c, BNU-ESM captures the observed feature of the FWF climatological seasonal cycle (Fig. 6a), i.e., a positive FWF anomaly occurs in the equatorial Pacific from January to March and a negative FWF anomaly for the rest of the year. Furthermore, BNU-ESM also reproduces the observed semi-annual variability. However, the transition from positive to negative anomaly happens a month later in the simulated field than the observed; the FWF variability in the model is stronger than observed, and the maximum FWF anomaly occurs in the eastern Pacific in May, instead of March as observed.

For the SSS climatological seasonal cycle along the equator, BNU-ESM (Fig. 6d) reproduces some of the observed features (Fig. 6b), e.g., the positive SSS anomalous water mass drifts from the western equatorial Pacific to the eastern equatorial Pacific; meanwhile, during the first half of the year (January–May), a negative SSS anomaly is observed in the eastern equatorial Pacific and, in the second half of the year, a positive SSS anomaly in the western equatorial Pacific.

However, the BNU-ESM simulation does contain some biases. For example, the variability of the SSS anomaly is weaker than observed, and the drift of the positive SSS anomaly is slower than observed, from the western equatorial Pacific to the eastern equatorial Pacific, leading to a stronger than observed positive SSS anomaly. Furthermore, the area of the positive anomaly is larger than observed in the western Pacific, resulting in a positive SSS anomaly simulated by BNU-ESM across the dateline, farther west compared to observations, and the area of the positive SSS anomaly is larger than observed in the latter half of the year in the central-eastern equatorial Pacific.

In general, BNU-ESM shows a pattern with semiannual variability, which cannot be observed in reality. It shows that the climatological seasonal cycle of SSS could be influenced not only by FWF but also by other oceanic processes.

3.2. *Interannual variability*

3.2.1. *Total fields*

The interannual variations of total FWF and SSS fields along the equator are shown in Fig. 7. Fresh waters are evident in the far western equatorial Pacific, denoted as the fresh pool, and saline waters are located in the central basin with a front near the dateline, directly associated with a convergence of water masses. In general, positive FWF varies greatly on an interannual scale in the western equatorial Pacific, where fresh waters are found in fall and saline waters in spring (Fig. 7a). Interannual variations of SSS derived from the objective EN3_V2a data are associated with ENSO events (Fig. 7b), predominantly controlled by the air–sea interaction processes of winds, SST and the thermocline (e.g., Zhang and Busalacchi, 2009).

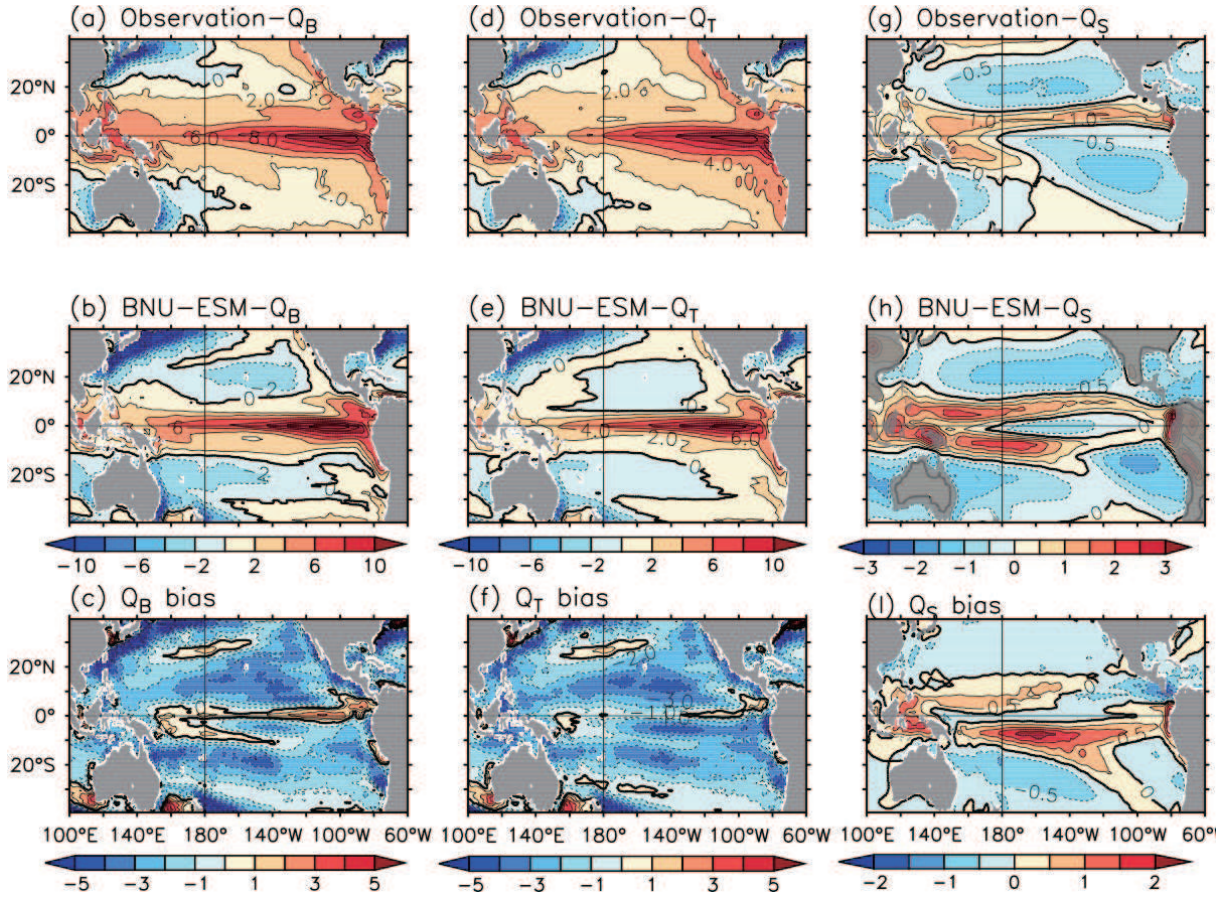

Fig. 5. Climatological distribution of buoyancy flux: total field (Q_B) (a) observed, (b) simulated by BNU-ESM, and (c) the model bias relative to observation; the heat flux part (Q_T) (d) observed, (e) simulated by BNU-ESM, and (f) the model bias; the freshwater flux part (Q_S) (g) observed, (h) simulated by BNU-ESM, and (l) the model bias relative to observation. Units: 1.0^{-5} kg m^{-2} s^{-1}.

Longitudinal displacements of large FWF (input into the surface) and SSS (higher than 34.8 psu) anomalies are evident along the equator. For example, during El Niño, the fresh water pool in the western equatorial Pacific extends eastward across the dateline and the saline water shrinks eastward along the equator across the dateline. In the equatorial area, the SSS front also moves back and forth with ENSO events (Fig. 7b). A freshening is seen in the western-central basin, accompanied by an extension of the fresh pool eastward across the dateline during El Niño.

BNU-ESM can simulate the corresponding interannual relationship observed between FWF and SSS (Figs. 7c and d). Fresh waters are evident in the far western equatorial Pacific, and saline waters are located in the central basin with a front near the dateline.

3.2.2. *Interannual anomalies*

Figures 8a and b show the interannual FWF and SSS anomalies observed along the equator. In terms of spatiotemporal structure, FWF varies most in the central-western equatorial Pacific (Fig. 8a), while large SSS variability higher than 0.2 psu occurs in the western-central basin (Fig. 8b). The SSS interannual variation shows a standing horizontal pattern concentrated around the dateline in the western-central equatorial Pacific, where the FWF also has large variability (e.g., Zhang and Busalacchi, 2009). During El Niño, the anomalous FWF is positive and higher than 2×10^{-5} kg m^{-2} s^{-1} and the anomalous SSS is negative and lower than -0.2 psu in the central and western basin. During the evolution from an El Niño to a La Niña phase, the FWF anomaly changes from higher than 2×10^{-5} kg m^{-2} s^{-1} to lower than -2×10^{-5} kg m^{-2} s^{-1}, and the SSS changes from a higher than -0.2 psu to a lower than 0.2 psu anomaly in the central equatorial Pacific, as noted by Zheng and Zhang (2012).

As shown in Figs. 8c and d, BNU-ESM can realistically simulate FWF (Fig. 8c) and SSS (Fig. 8d) interannual anomalies along the equator. The distinct FWF and SSS interannual anomalies are seen in the equatorial Pacific, but some differences exist between observations and the BNU-ESM simulation. For example, the stronger positive FWF anomaly (much higher than 4.0×10^{-5} kg m^{-2} s^{-1}) simulated by BNU-ESM is located in the western-central equatorial regions, which extends to 140°W farther eastward than observed. As a result, the negative SSS anomaly (lower than -0.6 psu) simulated in the western-central equatorial Pacific is stronger than observed, while the negative SSS anomaly simulated by

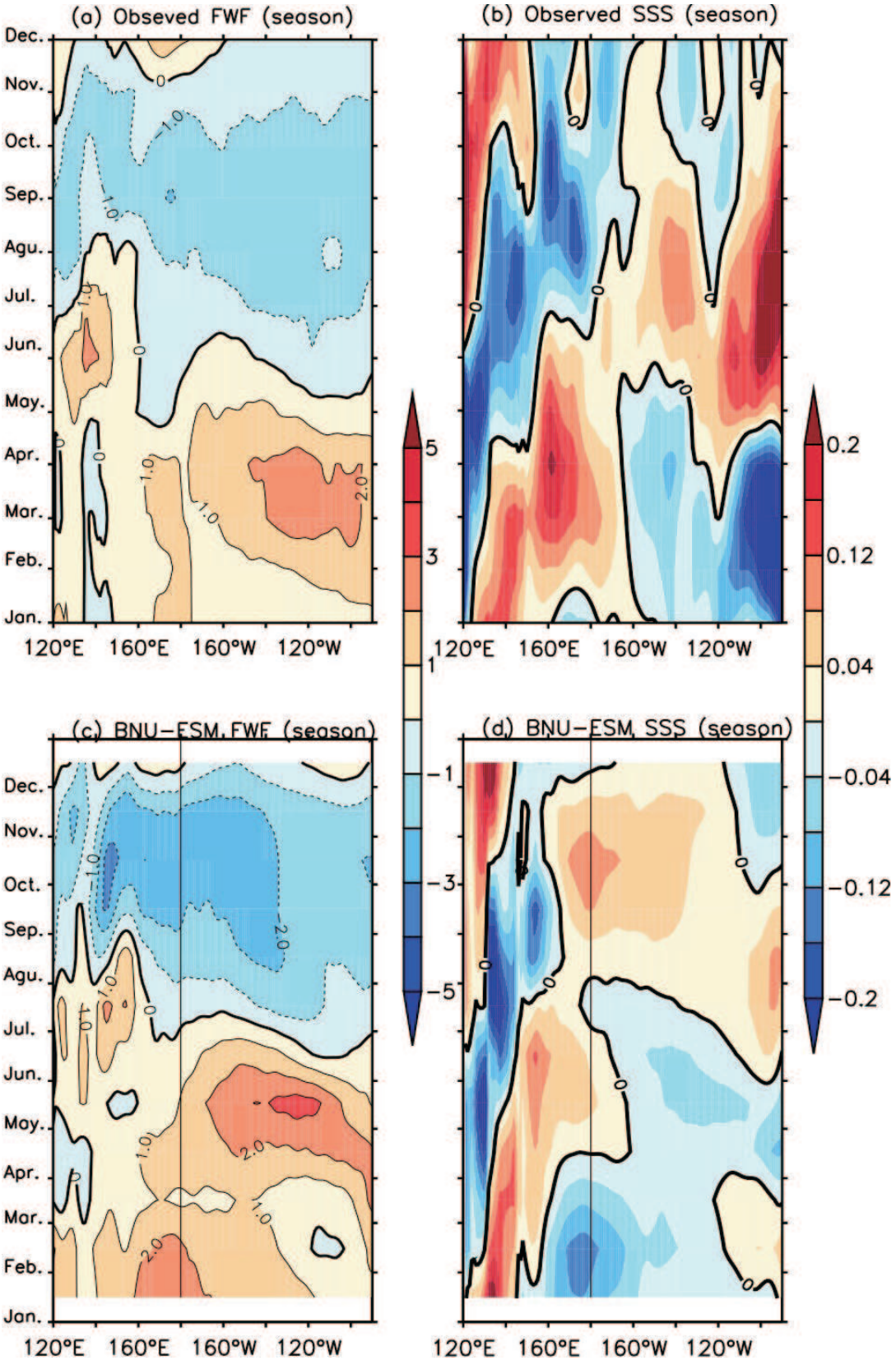

Fig. 6. Longitude–time sections of the climatological seasonal cycle along the equator (averaged between 2°N and 2°S) for (a) FWF and (b) SSS derived from EN3_V2a data; and (c) FWF and (d) SSS simulated by BNU-ESM. Units: 10^{-5} kg m^{-2} s^{-1} (for FWF) and psu (for SSS).

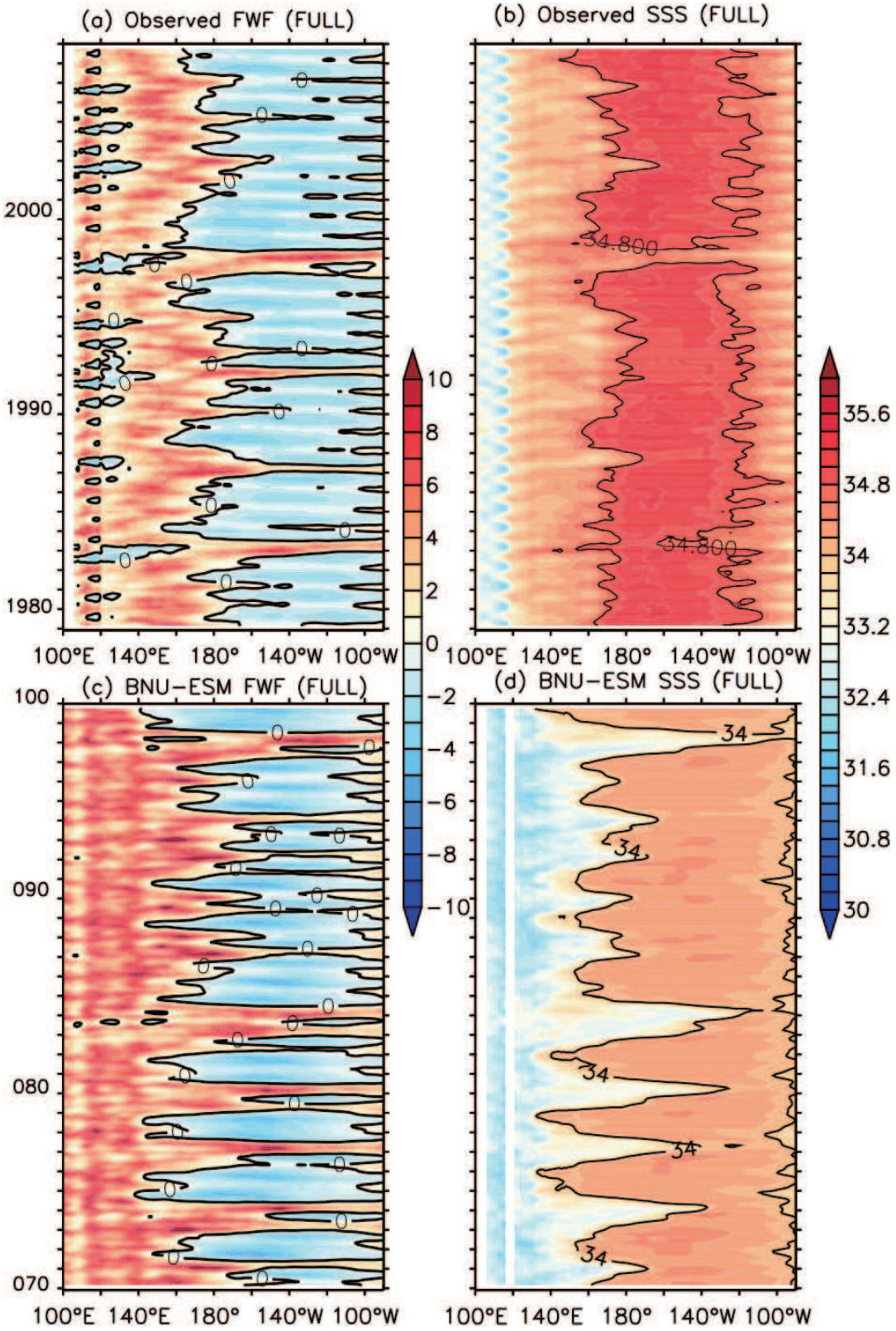

Fig. 7. Longitude–time sections of full fields along the equator (averaged between 2°N and 2°S) for (a) FWF and (b) SSS derived from EN3_V2a data; and (c) FWF and (d) SSS simulated by BNU-ESM. Units: 10^{-5} kg m^{-2} s^{-1} (for FWF) and psu (for SSS). The black line in (b) indicates the 34.8 psu isohaline, serving as the position of the salinity front as observed, and the black line in (d) indicates the 34.0 isohaline simulated by BNU-ESM. The *y*-coordinates of (c) and (d) are the last 30 year of 100 model year.

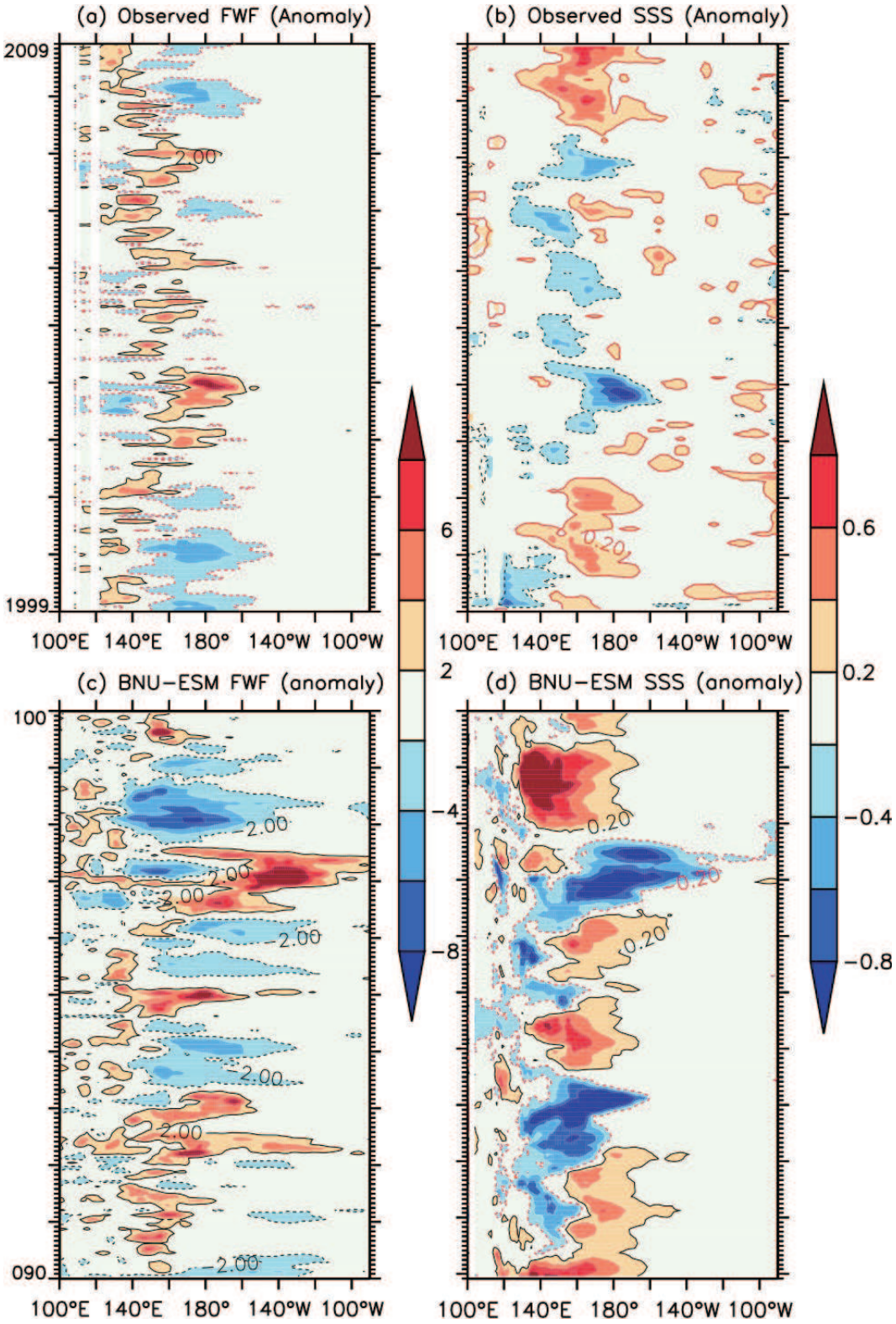

Fig. 8. Longitude–time sections of anomalies along the equator (averaged between 2°N and 2°S) for (a) FWF and (b) SSS derived from EN3_V2a data; and (c) FWF and (d) SSS simulated by BNU-ESM. Units: 10^{-5} kg m^{-2} s^{-1} (for FWF) and psu (for SSS). The *y*-coordinates of (c) and (d) are the last 10 year of 100 model year.

BNU-ESM in the western-central equatorial Pacific extends to 140°W farther eastward than observed.

The total fields of both observations and the simulation are demonstrated in Fig. 7 and the corresponding interan-

nual anomaly fields are shown in Fig. 8. The simulated FWF shows a larger interannual variation and a higher frequency crossing the dateline than in observations. Correspondingly, a stronger FWF interannual variation simulated by BNU-ESM is related to the stronger SSS interannual variability in the equatorial Pacific.

3.3. *Regression analysis*

In order to more clearly depict the relationships among the interannual anomalies of different variables, a regression analysis is conducted for interannual anomalies of SST, SSS, MLD, and the Q_B components (i.e., Q_B, Q_T and Q_S) during ENSO cycles. The dominant pattern for interannual SST variability is extracted using empirical orthogonal functions (EOFs). Then, the SST spatial pattern and corresponding time coefficient are obtained from EOF1. The observed variance contribution is about 48%, while the simulated variance contribution is about 27%. This represents the SST interannual pattern associated with ENSO. Using the SSTA PC1 (first principle component), we obtain the spatial distribution of some related fields using the regression analysis, including SSS, MLD and Q_B. The first spatial pattern for SST and the regressive spatial patterns for various observed anomaly fields are shown in Fig. 9. During warm events, a positive SST anomaly appears in the central-eastern basin (Fig. 9a), accompanied by a large positive FWF anomaly in the western-central equatorial Pacific, the SPCZ and ITCZ (Fig. 9b). The direct effect of the positive FWF anomaly leads to an increase in the negative SSS anomaly (Fig. 9c) in the western-central Pacific. Correspondingly, the surface ocean density becomes smaller. Accompanied by this, the MLD becomes shallower in the western-central equatorial Pacific, suppressing the entrainment of subsurface water into the mixed layer (Fig. 9d). At the same time, as a response to the positive FWF in the western-central Pacific, Q_S becomes a positive anomaly. Since Q_T and Q_S are negatively correlated with each other during the ENSO cycle, their effects on Q_B tend to be compensated. Thus, as part of Q_B, the positive Q_S anomaly acts to compensate for the negative Q_T anomaly (Fig. 9f), leading to a less negative Q_B anomaly (Fig. 9g). This reduced negative Q_B anomaly tends to decrease the MLD in the western-central equatorial region (Fig. 9d). These oceanic processes are favorable for warming in the surface layer, as previously demonstrated by Zhang and

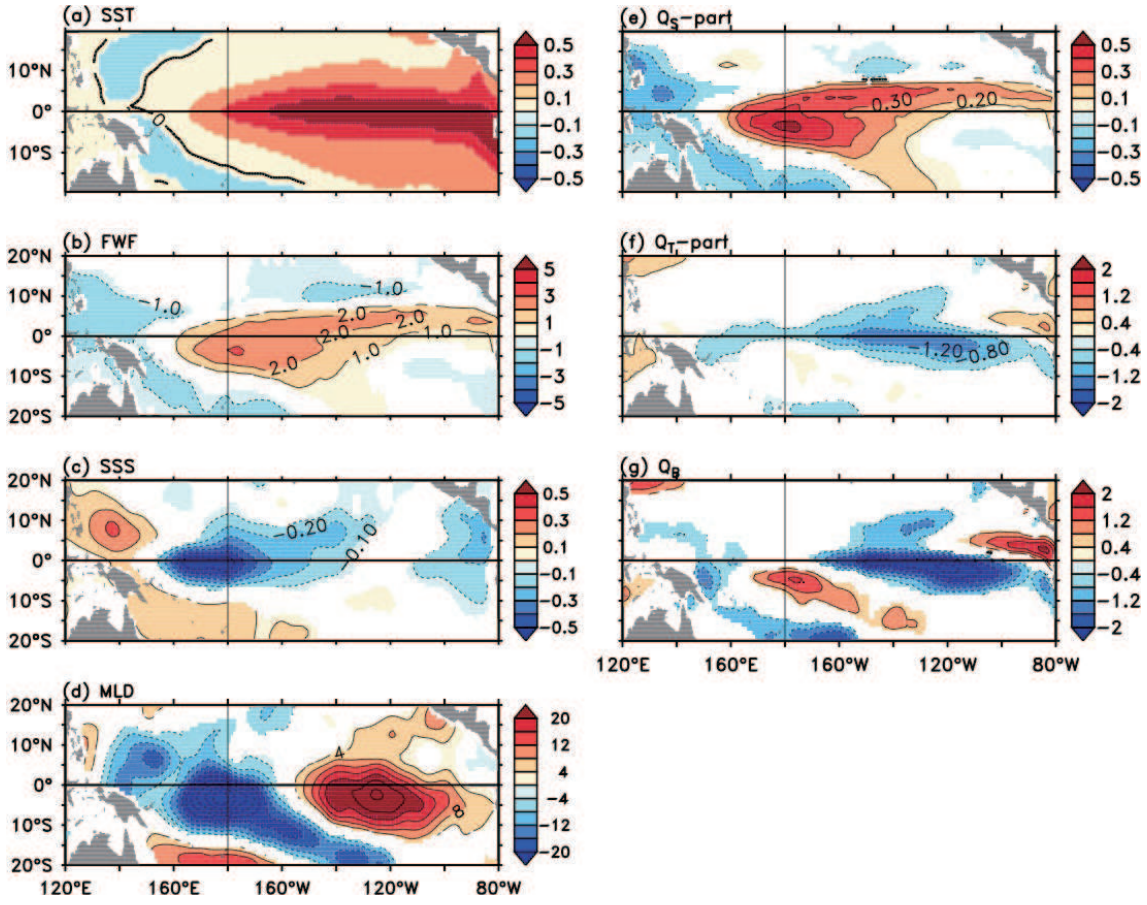

Fig. 9. (a) SST EOF1 and the regressive spatial patterns of the related ocean fields in the equatorial regions for the observation: (b) FWF; (c) SSS; (d) MLD; (e) the Q_S part; (f) the Q_T part; (g) Q_B. The contour intervals are 0.2°C in (a), 0.4×10^{-5} kg m^{-2} s^{-1} (°C)$^{-1}$ in (b), 0.1 psu (°C)$^{-1}$ in (c), 2.0 m (°C)$^{-1}$ in (d), 0.1×10^{-5} kg m^{-2} s^{-1} (°C)$^{-1}$ in (e), 0.2×10^{-5} kg m^{-2} s^{-1} (°C)$^{-1}$ in (f), and 0.4×10^{-5} kg m^{-2} s^{-1} (°C)$^{-1}$ in (g). The colored areas in (b–g) are statistically significant at the 99% confidence level.

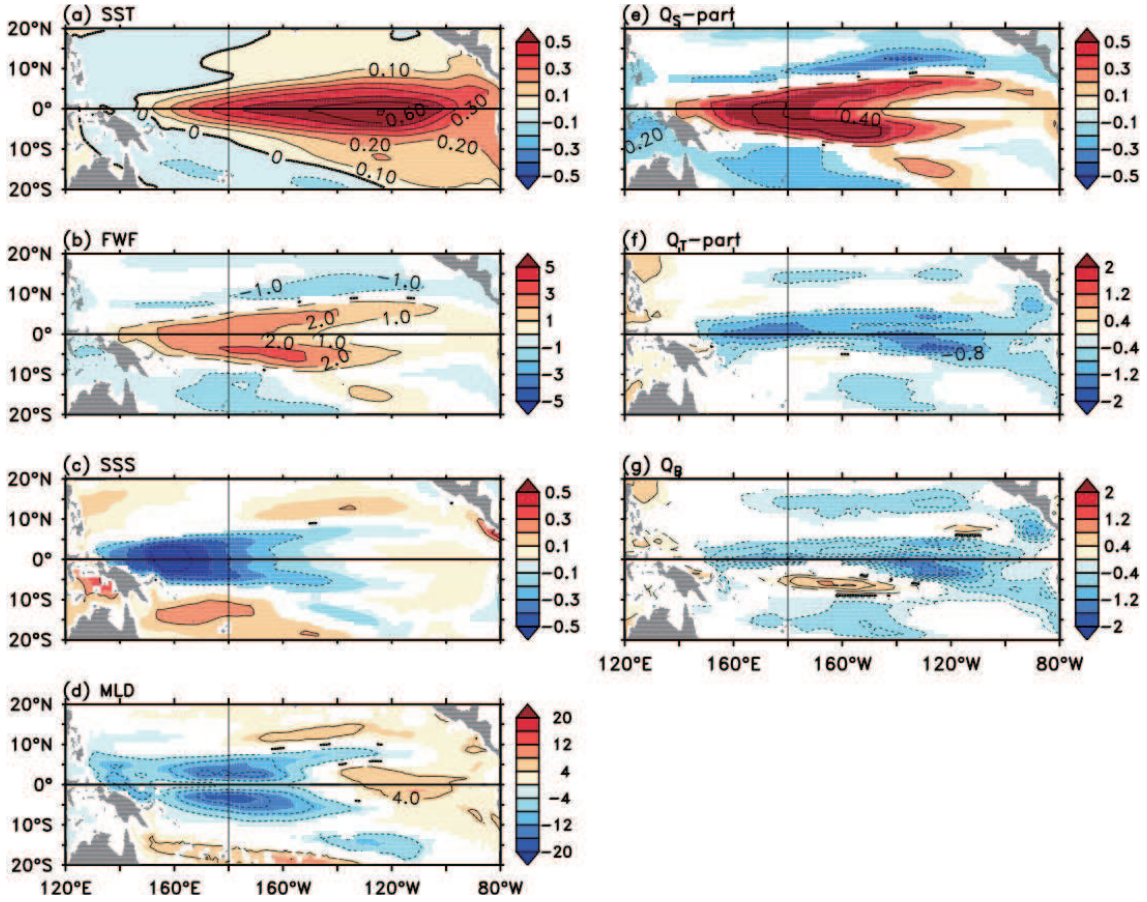

Fig. 10. As in Fig. 9 but for the BNU-ESM simulation. The colored areas in (b–g) are statistically significant at the 99% confidence level.

Busalacchi (2009).

The corresponding anomaly fields simulated by BNU-ESM are shown in Fig. 10. As observed, the SST EOF1 simulated by BNU-ESM also represents the ENSO mode (Fig. 10a). For example, during El Niño, there is more FWF into the ocean in the western-central equatorial Pacific (Fig. 10b), corresponding to the larger negative SSS anomaly (Fig. 10c). The high FWF into the ocean causes a lower surface density simulation by BNU-ESM, making the upper ocean more stable and thus suppressing cold water movement into the mixed layer (Fig. 10d). This results in stronger warming of SST during El Niño events. Therefore, these analyses can be utilized to illustrate positive feedback between FWF and SST during ENSO cycles, through the corresponding relationships among SSS, MLD, and Q_B. ENSO cycles are characterized by SST anomalies over the equatorial regions, which induce a pronounced FWF feedback effect on SST in the western-central basin (Zhang and Busalacchi, 2009).

As shown in Figs. 8c and d, BNU-ESM simulates the interannual anomalies of FWF and SSS along the equator well. However, some differences exist between observations and the BNU-ESM simulation. For example, the strong positive FWF anomaly simulated by BNU-ESM is located in the western-central equatorial regions, which extends farther eastward than observed. As a result, the negative SSS anomaly simulated in the western-central equatorial Pacific is stronger than observed, while the negative SSS anomaly simulated by BNU-ESM in the western-central equatorial Pacific extends farther eastward than observed.

4. Concluding remarks

FWF, as an ocean forcing through its direct effect on SSS, can change ocean thermal structure and other ocean fields, acting to modulate SST in the tropical Pacific. These physical processes have been previously analyzed and illustrated using simplified coupled ocean–atmosphere models (e.g., Zhang and Busalacchi, 2009; Zheng and Zhang, 2012). The salinity effects and related FWF forcing are found to have a close association with interannual variability in the tropical Pacific.

The main purpose of this paper is to assess BNU-ESM performance in terms of its simulations of mean climatology and variations of FWF and salinity fields in the tropical Pacific. A comparison between the BNU-ESM simulation and observation has been made to analyze FWF-related physical processes. For climatological annual mean fields, large FWFs into the ocean are mainly located in the far western equatorial Pacific, as represented by the fresh pool in the ocean; saline waters are located in the central basin with a front near the dateline, directly associated with a convergence of water

masses. The relatively shallower MLD in the western equatorial Pacific is associated with the lower SSS in the warm pool. At the same time, as one part of Q_B, a large FWF into the ocean in the western-central regions tends to compensate for HF, leading to significant modulations of Q_B. On an interannual time scale, SSS has large variations in response to the FWF anomaly in the western equatorial Pacific. The relationships among interannual variations in SST, FWF and SSS evolve during the ENSO cycle. BNU-ESM is able to reproduce the FWF-induced oceanic dynamic processes, a positive feedback on ENSO intensity.

The spatial distributions of SSS and the related oceanic fields simulated by BNU-ESM, including SST, MLD and Q_B, agree well with observations. However, positive FWF bias simulated by BNU-ESM is seen in the western-central tropical Pacific, particularly over the ITCZ and SPCZ. Based on the relationships between FWF and related physical fields, FWF bias simulated by BNU-ESM is clearly reflected in SSS and SST simulations. In the western equatorial Pacific, for example, a strong FWF anomaly corresponds to a low SSS and a small surface ocean density in the warm pool. Also, a strong FWF anomaly acts to compensate more for an HF anomaly, leading to a large modulation of Q_B, which tends to reduce the MLD. These related processes act to stabilize the upper ocean and depress mixing at the base of the mixed layer. As such, the FWF-induced positive feedback effect on SST simulated by BNU-ESM is stronger than observed during ENSO cycles. These process-oriented analyses provide guidance to improve BNU-ESM.

In addition, the biases between the BNU-ESM simulations and observations identified in this paper also require more objective analyses, because the quantity of observational data is poor in the comparison. For example, due to the lack of observations in the ocean, most data are reanalysis products, except for a few observations. Although the ARGO data have a wide range of applications in studying climate, their length is short, as the quality is high only after 2005. So, in terms of the performance of BNU-ESM in the PI control case, ARGO-based observations are not suitable for adequately assessing the biases of the BNU-ESM simulations. These issues need to be addressed in future work.

Acknowledgements. The authors wish to thank the anonymous reviewers for their numerous comments that helped to improve the original manuscript. Thanks also go to the modeling groups participating in CMIP5, and the PCMDI (Program For Climate Model Diagnosis and Intercomparison) for generously making available the model output used in this paper. This study was supported by the National Natural Science Foundation of China (NSFC) (Grant Nos. 41376039, 41376019, and 41475101), the NSFC–Shandong Joint Fund for Marine Science Research Centers (Grant No. U1406401), the NSFC Innovative Group Grant (Project No. 41421005), and the IOCAS [Institute of Oceanology, Chinese Academy of Sciences (CAS)] through the CAS Strategic Priority Project [Western Pacific Ocean System (WPOS)]. This is publication No. 048 of the Earth System Modeling Center (ESMC), supported by the Joint Center for Global Change Studies (Project No. 105019) and the Key Laboratory of Meteorological Disaster of Ministry of Education, NUIST (Nanjing University of Information Science & Technology) (Grant No. KLME 1311), and the Priority Academic Program Development (PAPD) of Jiangsu Higher Education Institutions.

REFERENCES

Adler, R. F., and Coauthors, 2003: The version-2 global precipitation and climatology project (GPCP) monthly precipitation analysis (1979–present). *Journal of Hydrometeorology*, **4**, 1147–1167.

Bellenger, H., E. Guilyardi, J. Leloup, M. Lengaigne, and J. Vialard, 2014: ENSO representation in climate models: From CMIP3 to CMIP5. *Climate Dyn.*, **42**, 1999–2018.

Cravatte, S., T. Delcroix, D. X. Zhang, M. McPhaden, and J. Leloup, 2009: Observed freshening and warming of the western Pacific Warm Pool. *Climate Dyn.*, **33**, 565–589.

Delcroix, T., and C. Hénin, 1991: Seasonal and interannual variations of sea surface salinity in the tropical Pacific Ocean. *J. Geophys. Res.*, **96**, 22 135–22 150.

Delcroix, T., S. Cravatte, and M. J. McPhaden, 2007: Decadal variations and trends in tropical Pacific sea surface salinity since 1970. *J. Geophys. Res.*, **112**, C03012, doi: 10.1029/2006JC 003801.

Fedorov, A. V., R. C. Pacanowski, S. G. Philander, and G. Boccaletti, 2004: The effect of salinity on the wind-driven circulation and the thermal structure of the upper ocean. *J. Phys. Oceanogr.*, **34**, 1949–1966.

Fettweis, X., E. Hanna, C. Lang, A. Belleflamme, M. Erpicum, and H. Gallée, 2013: Brief communication "Important role of the mid-tropospheric atmospheric circulation in the recent surface melt increase over the Greenland ice sheet". *The Cryosphere*, **7**, 241–248.

Fujii, Y., M. Kamachi, S. Matsumoto, and S. Ishizaki, 2012: Barrier layer and relevant variability of the salinity field in the equatorial Pacific estimated in an ocean reanalysis experiment. *Pure Appl. Geophys.*, **169**, 579–594.

Guinehut, S., C. Coatanoan, A.-L. Dhomps, P.-Y. Le Traon, and G. Larnicol, 2009: On the use of satellite altimeter data in Argo quality control. *J. Atmos. Oceanic Technol.*, **26**, 395–402.

Hackert, E., J. Ballabrera-Poy, A. J. Busalacchi, R.-H. Zhang, and R. Murtugudde, 2011: Impact of sea surface salinity assimilation on coupled forecasts in the tropical Pacific. *J. Geophys. Res.*, **116**, C05009, doi: 10.1029/2010JC006708.

Hackert, E., A. J. Busalacchi, and J. Ballabrera-Poy, 2014: Impact of Aquarius sea surface salinity observations on coupled forecasts for the tropical Indo-Pacific Ocean. *J. Geophys. Res.: Oceans*, **119**(7), 4045–4067.

Ham, S., S.-Y. Hong, Y. Noh, S.-II An, Y.-H. Byun, H.-S. Kang, J. Lee, and W.-T. Kwon, 2012: Effects of freshwater runoff on a tropical Pacific climate in the HadGEM2. *Asia-Pacific Journal of Atmospheric Sciences*, **48**(4), 457–463.

Han, W. Q., J. P. McCreary Jr., and K. E. Kohler, 2001: Influence of precipitation minus evaporation and Bay of Bengal rivers on dynamics, thermodynamics, and mixed layer physics in the upper Indian Ocean. *J. Geophys. Res.*, **106**, 6895–6916.

Howden, S. D., and R. Murtugudde, 2001: Effects of river inputs into the Bay of Bengal. *J. Geophys. Res.*, **106**, 19 825–19 843.

Huang, B. Y., and V. M. Mehta, 2005: Response of the Pacific and Atlantic oceans to interannual variations in net atmospheric freshwater. *J. Geophys. Res.*, **110**, C08008, doi: 10.1029/2004

JC002830.

Ji, D., and Coauthors, 2014: Description and basic evaluation of BNU-ESM version1. *Geoscientific Model Development*, **7**, 1601–1647.

Kang, X. B., R. H. Huang, Z. G. Wang, and R.-H. Zhang, 2014: Sensitivity of ENSO variability to Pacific freshwater flux adjustment in the Community Earth System Model. *Adv. Atmos. Sci.*, **31**(5), 1009–1021, doi: 10.1007/s00376-014-3232-2.

Levitus, S., 1983: *Climatological Atlas of the World Ocean.* U.S. Government Printing Office, 173 pp.

Lin, J.-L., 2007: The double-ITCZ problem in IPCC AR4 coupled GCMs: Ocean-atmosphere feedback analysis. *J. Climate*, **20**, 4497–4525.

Lin, P. F., Y. Q. Yu and H. L. Liu, 2013a: Long-term stability and oceanic mean state simulated by the coupled model FGOALS-s2. *Adv. Atmos. Sci.*, **30**, 175–192, doi: 10.1007/s00376-012-2042-7.

Lin, P. F., Y. Q. Yu and H. L. Liu, 2013b: Oceanic climatology in the coupled model FGOALS-g2: Improvements and biases. *Adv. Atmos. Sci.*, **30**, 819–840, doi: 10.1007/s00376-012-2137-1.

Lukas, R., and E. Lindstrom, 1991: The mixed layer of the western equatorial Pacific Ocean. *J. Geophys. Res.*, **96**, 3343–3357.

Ma, H., L. X Wu, Z. Q. Li, 2013: Impact of freshening over the Southern Ocean on ENSO. *Atmospheric Science Letters*, **14**(1), 28–33.

Maes, C., 2000: Salinity variability in the equatorial Pacific Ocean during the 1993–98 period. *Geophys. Res. Lett.*, **27**, 1659–1662.

Maes, C., J. Picaut, and S. Belamari, 2002: Salinity barrier layer and onset of El Niño in a Pacific coupled model. *Geophys. Res. Lett.*, **29**(24), 59-1–59-4, doi: 10.1029/2002GL016029.

Mechoso, C. R., and Coauthors, 1995: The seasonal cycle over the tropical Pacific in coupled ocean-atmosphere general circulation models. *Mon. Wea. Rev.*, **123**, 2825–2838.

Murtugudde, R., and A. J. Busalacchi, 1998: Salinity effects in a tropical ocean model. *J. Geophys. Res.*, **103**, 3283–3300.

Rao, R. R., and K. V. Sanil Kumar, 1991: Evolution of salinity field in the upper layers of the east central Arabian Sea and northern Bay of Bengal during summer monsoon experiments. *Proceedings of the Indian Academy of Sciences-Earth and Planetary Sciences*, **100**, 69–78.

Rao, R. R., and R. Sivakumar, 1999: On the possible mechanisms of the evolution of a mini-warm pool during the pre-summer monsoon season and the genesis of onset vortex in the South-Eastern Arabian Sea. *Quart. J. Roy. Meteor. Soc.*, **125**, 787–809.

Schiffer, R. A., and W. B. Rossow, 1985: ISCCP global radiance data set: a new resource for climate research. *Bull. Amer. Meteor. Soc.*, **66**, 1498–1505.

Sévellec, F., and A. V. Fedorov, 2011: Stability of the Atlantic meridional overturning circulation and stratification in a zonally averaged ocean model: Effects of freshwater flux, Southern Ocean winds, and diapycnal diffusion. *Deep Sea Research Part II: Topical Studies in Oceanography*, **58**, 1927–1943.

Sprintall, J., and M. Tomczak, 1992: Evidence of the barrier layer in the surface layer of the tropics. *J. Geophys. Res.*, **97**, 7305–7316.

Taylor, K. E., R. J. Stouffer, and G. A. Meehl, 2012: An overview of CMIP5 and the experiment design. *Bull. Amer. Meteor. Soc.*, **93**, 485–498.

Thompson, B., C. Gnanaseelan, and P. S. Salvekar, 2006: Variability in the Indian Ocean circulation and salinity and its impact on SST anomalies during dipole events. *J. Mar. Res.*, **64**, 853–880.

Webster, P. J., 1994: The role of hydrological processes in ocean-atmosphere interactions. *Rev. Geophys.*, **32**, 427–476.

Wu, L. X., Y. Sun, J. X. Zhang, L. P. Zhang, and S. Minobe, 2010: Coupled ocean-atmosphere response to idealized freshwater forcing over the western tropical Pacific. *J. Climate*, **23**(7), 1945–1954.

Wu, R. G., J. P. Chen, and Z. P. Wen, 2013: Precipitation-surface temperature relationship in the IPCC CMIP5 Models. *Adv. Atmos. Sci.*, **30**, 766–778, doi: 10.1007/s00376-012-2130-8.

Yang, S., K.-M. Lau, and P. S. Schopf, 1999: Sensitivity of the tropical Pacific Ocean to precipitation-induced freshwater flux. *Climate Dyn.*, **15**, 737–750.

Yu, L. S., 2011: A global relationship between the ocean water cycle and near-surface salinity. *J. Geophys. Res.*, **116**, C10025, doi: 10.1029/2010JC006937.

Yu, L. S., and R. A. Weller, 2007: Objectively analyzed air-sea heat fluxes for the global ice-free oceans (1981–2005). *Bull. Amer. Meteor. Soc.*, **88**, 527–539.

Zhang, L. P., C. Z Wang, and S.-K. Lee, 2014: Potential role of Atlantic Warm Pool-induced freshwater forcing in the Atlantic Meridional Overturning Circulation: Ocean-sea ice model simulations. *Climate Dyn.*, **43**, 553–574.

Zhang, R.-H., and A. J. Busalacchi, 2009: Freshwater flux (FWF)-induced oceanic feedback in a hybrid coupled model of the tropical Pacific. *J. Climate*, **22**, 853–879.

Zhang, R.-H., A. J. Busalacchi, R. G. Murtugudde, P. A. Arkin, and J. Ballabrera-Poy, 2006: An empirical parameterization for the salinity of subsurface water entrained into the ocean mixed layer (S_e) in the tropical Pacific. *Geophys. Res. Lett.*, **33**, L02605, doi: 10.1029/2005GL024218.

Zhang, R.-H., G.H. Wang, D. K. Chen, A. J. Busalacchi, and E. C. Hackert, 2010: Interannual biases induced by freshwater flux and coupled feedback in the tropical Pacific. *Mon. Wea. Rev.*, **138**, 1715–1737.

Zhang, R.-H., F. Zheng, J. S. Zhu, Y. H. Pei, Q. A. Zheng, and Z. G. Wang, 2012: Modulation of El Niño-Southern Oscillation by freshwater flux and salinity variability in the tropical Pacific. *Adv. Atmos. Sci.*, **29**, 647–660, doi: 10.1007/s00376-012-1235-4.

Zhang, R.-H., F. Zheng, J. Zhu, and Z. G. Wang, 2013: A successful real-time forecast of the 2010–11 La Nina event. *Sci. Rep.* **3**, 1108; DOI: 10.1038/srep01108.

Zheng, F., and R.-H. Zhang, 2012: Effects of interannual salinity variability and freshwater flux forcing on the development of the 2007/08 La Niña event diagnosed from Argo and satellite data. *Dyn. Atmos.* (*Oceans*), **57**, 45–57.

Zheng, F., R.-H. Zhang, and J. Zhu, 2014: Effects of interannual salinity variability on the barrier layer in the western-central equatorial Pacific: A diagnostic analysis from Argo. *Adv. Atmos. Sci.*, **31**, 532–542, doi: 10.1007/s00376-013-3061-8.